SCIENCE CHINA
Earth Sciences

• RESEARCH PAPER •

January 2011 Vol.54 No.1: 136–144
doi: 10.1007/s11430-010-4126-5

New eolian red clay sequence on the western Chinese Loess Plateau linked to onset of Asian desertification about 25 Ma ago

QIANG XiaoKe[1], AN ZhiSheng[1*], SONG YouGui[1], CHANG Hong[1], SUN YouBin[1], LIU WeiGuo[1], AO Hong[1], DONG JiBao[1], FU ChaoFeng[2], WU Feng[1], LU FengYan[1], CAI YanJun[1], ZHOU WeiJian[1], CAO JunJi[1], XU XinWen[1] & AI Li[1]

[1] *State Key Laboratory of Loess and Quaternary Geology (SKLLQG), Institute of Earth Environment, Chinese Academy of Sciences, Xi'an 710075, China;*
[2] *Key Laboratory of Western Mineral Resources and Geological Engineering of Ministry of Education, Chang'an University, Xi'an 710065, China*

Received October 21, 2010; accepted November 5, 2010; published online November 30, 2010

The expansion of inland Asia deserts has considerably influenced the environmental, social and economic activities in Asia. Aridification of inland Asia, especially timing of the initiation of Asian desertification, is a contentious topic in paleoclimatology. Late Cenozoic eolian loess-red clay sequences on the Chinese Loess Plateau, which possess abundant paleoclimatic and paleo-environmental information, can be regarded as an indicator of inland Asia desertification. Here we present a detailed magnetostratigraphic investigation of a new red clay sequence about 654 m in Zhuanglang located at the western Chinese Loess Plateau. Sedimentological, geochemical, mineralogical, and quartz morphological lines of evidence show that the red clay is of eolian origin. Magnetostratigraphic correlations indicate that this core sequence spans from 25.6 to 4.8 Ma, and typical eolian red clay appears as early as 25 Ma. This extends the lower limit of the red clay on the Chinese Loess Plateau from the previously thought early Miocene back into the late Oligocene. This new red clay record further implies that the inland Asia desertification was initiated at least by the late Oligocene. This sequence provides a unique high-resolution geological record for understanding the inland Asia desertification process since the late Oligocene.

Chinese Loess Plateau, eolian red clay, magnetostratigraphy, late Oligocene, inland Asia desertification

Citation: Qiang X K, An Z S, Song Y G, et al. New eolian red clay sequence on the western Chinese Loess Plateau linked to onset of Asian desertification about 25 Ma ago. Sci China Earth Sci, 2011, 54: 136−144, doi: 10.1007/s11430-010-4126-5

The loess-paleosol sequences on the Chinese Loess Plateau (CLP) have drawn much attention from the world for its good continuity, high sedimentation rate, long time span, and rich paleoclimate information. In the 1960s, Liu and Zhang [1] documented the eolian origin of the Chinese loess and divided it as the early Pleistocene Wucheng Loess, the mid-Pleistocene Lishi Loess, and the late-Pleistocene Malan Loess. At the end of 1970s, Chinese researchers proposed the concept of loess-paleosol sequence according to the alternating occurrence of loess and paleosol layers [2, 3]. Based on this, the stratigraphy for the loess-paleosol sequence was further defined and labeled [2, 4–7]. In 1982, Heller and Liu [8] established a 2.5-Ma magnetostratigraphy for the Chinese loess-paleosol sequence, which shows good correlation with the marine oxygen isotope record [4, 6, 9–17]. In the early 1990s, An et al. [18, 19] suggested that the Quaternary loess-paleosol sequence documents the East Asian monsoon changes and that the dust flux variation

*Corresponding author (email: anzs@loess.llqg.ac.cn)

reflects the aridity changes in inland Asia [14]. Early this century, a 7-Ma history of the Asian aridification was reconstructed based on the dust flux estimated from the Lingtai loess-red clay sequence [20, 21].

Along with the extensive study of the Quaternary loess, the underlying red clay also attracted much attention from climatologists, geographers, and geologists. Similar to loess, the red clay was also proven to be of eolian origin [22–30]. The red clay sequences on the eastern CLP are generally younger than 8.5 Ma [31–39], with the exception of the Shilou sequence (Figure 1), which extends back to ca. 11 Ma [40]. On the western CLP, however, red clay sequences are normally older than 11 Ma, with the Qin'an sequence as old as 22 Ma [41]. These lines of evidence indicate that the desertification of inland Asia was initiated by the early Miocene. A new eolian red clay sediment as old as 24 Ma in

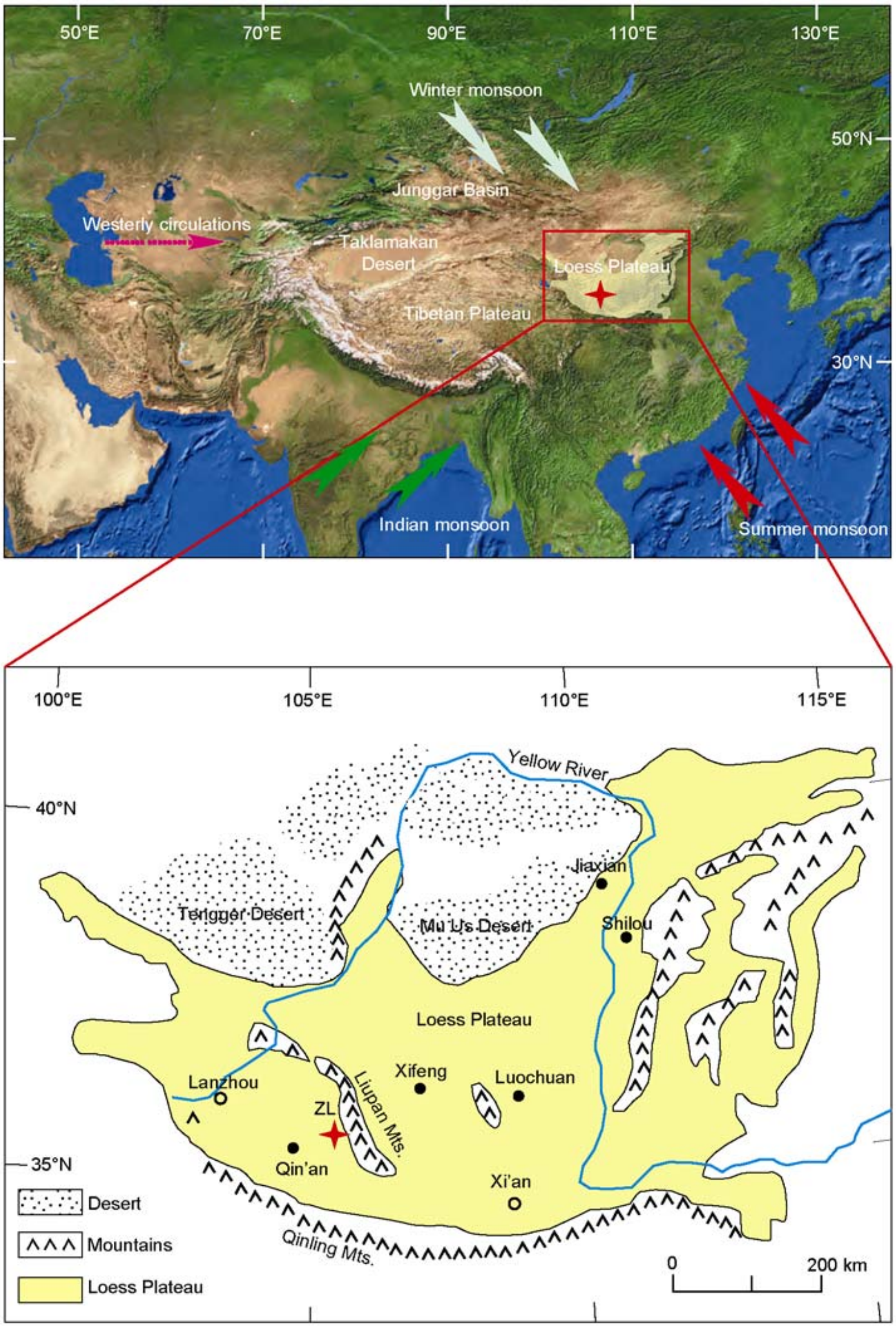

Figure 1 Locations of the Chinese Loess Plateau, the deserts in northern China and the Zhuanglang (ZL) drill site, and the atmospheric circulation system over China.

Junggar Basin was reported in this year [42]. Despite these studies, the earliest sequence on the CLP has not yet been proven, and it remains unclear to what extent eolian deposition is linked to the Asian desertification during the early periods. Recently, a thick continuous (>600 m) red clay sequence on the western CLP was found during the field investigation [43]. In this paper, we report the magnetostratigraphy and the evidence for the eolian origin of this new red clay sequence.

1 General settings and sampling

Zhuanglang (ZL) County (35°13′N, 106°05′E), on the western CLP, is 50 km northeast of Qin'an section [41] (Figure 1). At present, the mean annual temperature and precipitation at ZL are about 8°C and 500 mm, respectively. The red clay is widely distributed over the tablelands, and ridges in this area, but the outcrop is not complete. In order to get a continuous high-resolution record, the ZL drilling core is obtained, which consists of two parallel holes (with a distance of ca. 1.5 km): the main ZL1 core has a depth of 555.7 m with a top elevation of 1993 m and the parallel ZL2 core has a depth of 308.5 m with a top elevation of 1643 m. They were combined into the ZL core, based on lithology, magnetostratigraphy and magnetic susceptibility correlations. The composite ZL core has a depth of 653.9 m, with the upper 450.4 m from the upper ZL1 core and the lower 203.5 m from the lower ZL2 core. The composite ZL core can be divided into five lithologic units from bottom to top: (I) Proterozoic dark grey biotite gneiss (653.9–652.3 m). (II) Oligocene purplish-red to light-brown sandy gravels (652.3–624.8 m). (III) Alternating red clay and sand/gravel layers (628.3–584.7 m), red clay has clear aggregate-like silty structure with porphyritic carbonate nodule and dark coatings. (IV) Thick red clay (584.7–3.34 m) is characterized by alternative yellowish brown loess/weak paleosol and reddish brown paleosol horizons, without horizontal bedding. Paleosol shows aggregate-like structure and dark coatings. Porphyritic nodules are scattered on the bottom of paleosol horizon or top of loess/weak paleosol horizons. Several yellowish-brown to greyish-brown sand and gravel layers intercalated in the upper part of this interval (124.32–3.34 m). (V) Late Pleistocene Malan loess and cultivating layer (3.34 m to the top).

After being split and cleaned, U-channel samples (U-shaped, 2 cm × 2 cm square cross-section, 1.5 m in length, non-magnetic plastic tubing, with an arrow showing an "up" direction) were taken from one half of the split core for continuous long-core magnetic measurements. In total, 361 and 162 U-channel cores were taken from the ZL1 and ZL2 cores, respectively. In addition, 3670 and 1640 discrete samples (2 cm × 2 cm × 2 cm) were taken from ZL1 and ZL2 cores with a spacing of about 10–20 cm, respectively.

2 Magnetostratigraphy

Low-field magnetic susceptibility (χ, calculated on a mass-specific basis) was measured with a Bartington MS2 meter at a frequency of 470 Hz. Remanence was measured using a 2G cryogenic superconducting magnetometer (model 755R) housed in the magnetic shielded space (<150 nT) at the Institute of Earth Environment, Chinese Academy of Sciences. All the 523 U-channel cores were subjected to stepwise alternating field (AF) demagnetization at fields up to 80 mT with 5 or 10 mT increments (measuring space is 5 cm). All the 5310 discrete samples were subjected to stepwise thermal demagnetization using a TD-48 thermal demagnetizer. They were stepwise heated to 690°C, with temperature increments of 10–50°C. Demagnetization results were evaluated by orthogonal diagrams [44] and the principal components direction was computed using a "least-squares fitting" technique [45].

Most samples yielded a stable characteristic remnant magnetization (ChRM) component after stepwise AF demagnetization up to 80 mT or thermal demagnetization up to 585°C, which indicates that magnetite is the dominant carrier of ChRM. However, some samples had to be heated to 690°C in order to determine a stable ChRM component. This suggests the presence of high-coercivity hematite. More than four successive points in the orthogonal diagrams were used to calculate the direction of ChRM during the establishment of polarity sequence (Figure 2). Among the 5310 discrete samples, 4880 (92%) samples gave reliable ChRM directions. The AF and thermal demagnetizations resulted in an overall consistent change in the ChRM vector directions, except for some short intervals, because the 80-mT AF demagnetization is difficult to isolate a stable ChRM that is carried by hematite. Thus, the detailed geomagnetic polarity variations of the ZL1 and ZL2 cores were defined mainly by the thermal demagnetization isolated ChRM vector directions, with the consideration of AF demagnetization data. Results suggest that the ZL1 core recorded 39 normal and 39 reversal magnetozones, while the ZL2 core recorded 21 normal and 20 reversed magnetozones (Figure 3). The composite ZL core recorded 44 normal and 43 reversed magnetozones (Figure 4). This composite ZL magnetic polarity sequence can be calibrated to the Geomagnetic Polarity Time Scale (GPTS) [46], which implies that the ZL core has recorded a nearly continuous magnetic polarity sequence from C7An to C3n.3n, covering an age range from 25.6 to 4.8 Ma. The boundaries of Oligocene-Miocene (23.03 Ma) and Miocene-Pliocene (5.332 Ma) (International Stratigraphic Chart 2009) are located at 568 and 29 m depths of the composite ZL core, respectively. The occurrence of red clay at 624.8 m is located at the upper of C7n.2n normal subchron (ca. 24.85 Ma).

The magnetostratigraphy, magnetic susceptibility and lithology of the ZL core correlate well with those of the

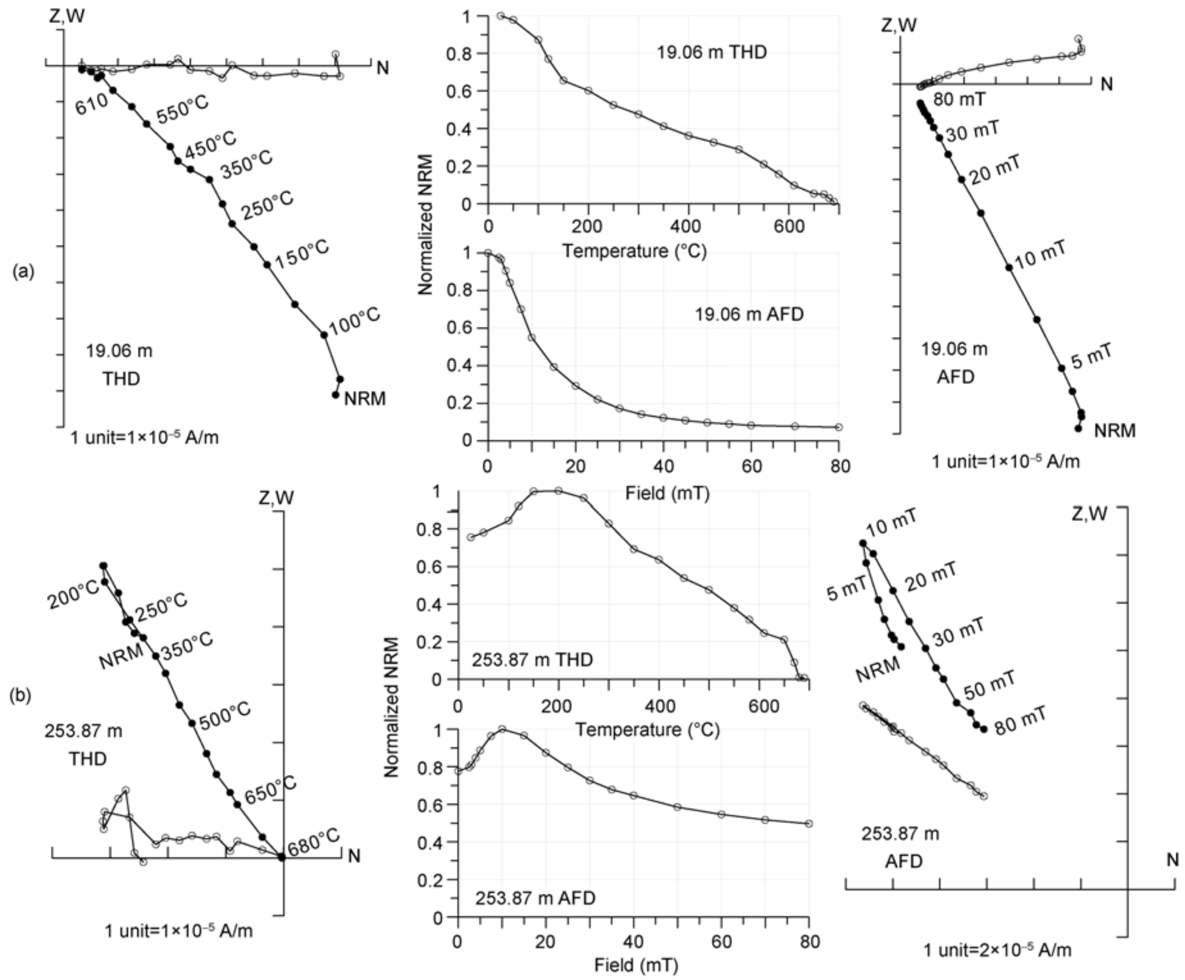

Figure 2 Orthogonal projections [44] of progressive thermal demagnetization (THD) and alternating field demagnetization (AFD) of NRM, and normalized intensity decay plots of ZL red clay. The solid (open) circles refer to the vertical (horizonta1) plane. (a) 19.06 m normal sample; (b) 253.87 m reversal sample.

Qin'an section [41] (Figure 4). In particular, their long-term changes of magnetic susceptibility are rather similar, with a notable high χ value interval between ca. 14 and 16 Ma (Figure 4). Note that the sedimentation rate of ZL red clay sequence is about twice higher than that of the Qin'an sequence. This may be due to their different geographical location. The ZL sequence is just located at the western flank of the Liupan Mountains, the windward slope, where is more prone to deposit thick eolian dust from inland Asia.

3 Evidence for the eolian origin

The red clay deposits on both the western and eastern CLP have been well documented to be of eolian origin [4, 24, 25, 40, 41, 47]. Outcrop and lithogically similar to the Qin'an section, the ZL red clay is composed with alternative loess/weak paleosol and paleosol horizon (including the underlain carbonate nodules). To further demonstrate the eolian origin of the ZL red clay sequence, we analyzed its grain-size distribution, element and mineral compositions, and quartz micromorphology. Grain-size analyses were performed on a Master Sizer 2000 laser spectrometer. Major elements were analyzed by X-ray fluorescence (XRF) using a Philips PW1400 unit. X-ray diffraction (XRD) analysis was carried out using an X'Pert Pro MPD X-ray diffractometer. Rare earth elements were analyzed by inductively coupled plasma-mass spectrometry (ICP-MS, Thermo Elemental X Series) in the Desert Research Institute, USA. Quartz micromorphology was observed by scanning electron microscope (SEM) using an LEO 1450VP unit.

Figure 5 shows the grain-size distribution, major and rare earth elements, mineral composition, and quartz micromorphology of selected samples from the ZL red clay sequence (including the bottom of the red clay sequence, 612.1–624.8 m) and their comparisons with those of typical Quaternary loess and Pliocene red clay samples. The ZL red clay and the Quaternary loess/paleosol samples from Luochuan (LC) and Xifeng (XF) (Figure 1) display similar curves of grain-size frequency and cumulative percentage distribution,

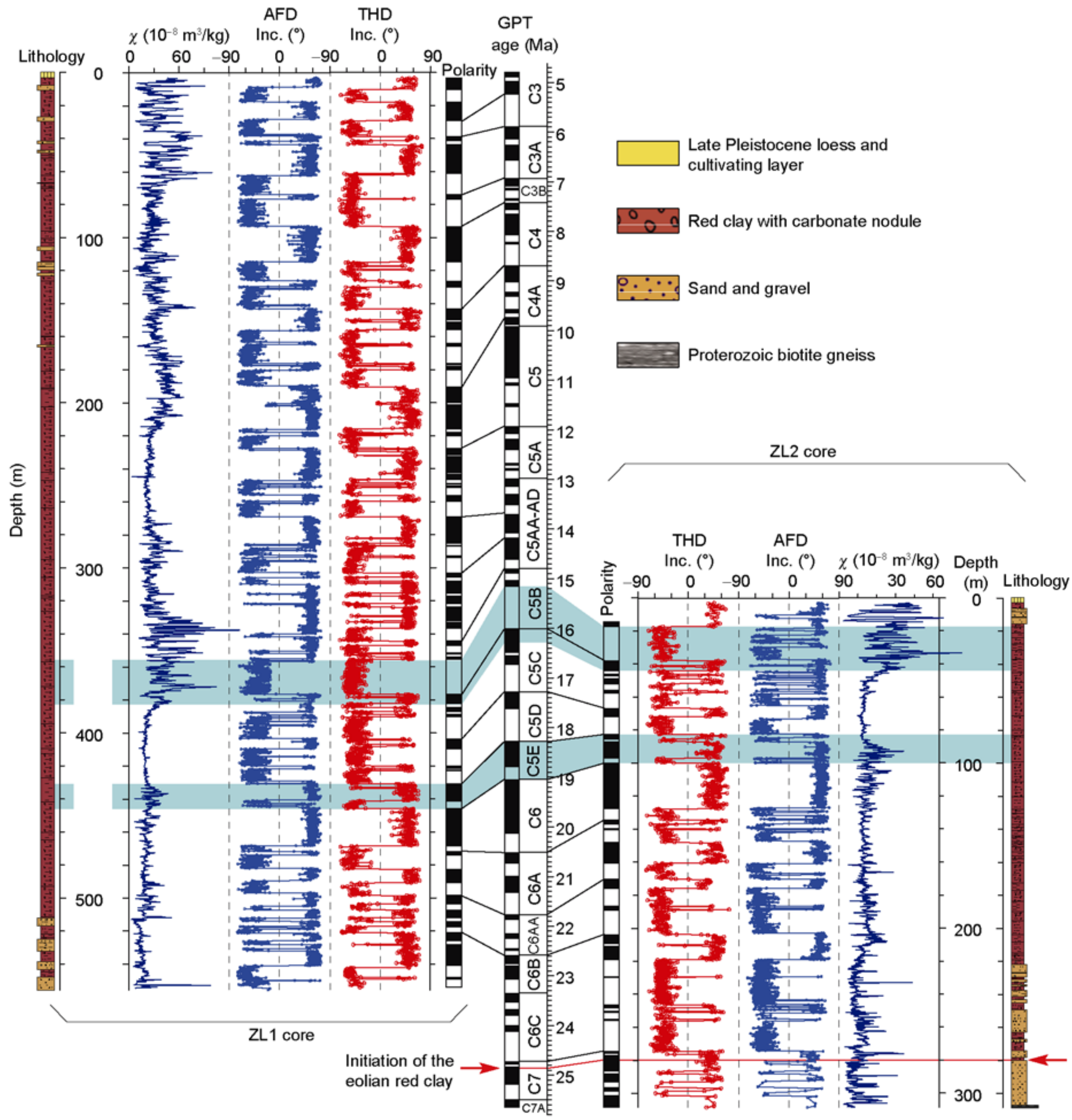

Figure 3 Lithostratigraphy, magnetic susceptibility (χ), and magnetostratigraphy of the ZL1 and ZL2 cores, and their comparison with Geomagnetic Polarity Time Scale (GPTS) [46]. AFD, alternating field demagnetization; THD, thermal demagnetization; Inc., inclination.

with a dominant silty fraction (4–63 μm) and a limited sandy fraction (>63 μm) (Figure 5(a) and (b)). The major element composition pattern of the ZL red clay and that of the LC Quaternary loess are nearly identical (Figure 5(c)). Similarly, the rare earth element distribution pattern of the ZL red clay and the XF Quaternary loess are consistent with each other (Figure 5(d)). The mineral composition of the ZL red clay also resembles those of the LC Quaternary loess and Pliocene XF red clay (Figure 5(e)), which is dominated by quartz, calcite and feldspar, with a few mica and chlorite. In addition, SEM observation indicates that most quartz particles are finer than 30 μm in diameter and have irregular and angular shapes with disk pit, sharp edges, and conchiform fractures (Figure 5(f)). All of these data strongly support eolian origin of the ZL red clay sequence.

4 Discussion and conclusion

It has been well documented that the dust materials of loess-red clay sequence on the CLP are derived mainly from the desert areas of the inland Asia through wind transport [4, 13, 48–50]. The similar grain-size distribution, element and mineral composition, quartz micromorphology, and lithology between the ZL red clay and the Quaternary loess/paleosol not only reveal the eolian origin of the ZL red clay,

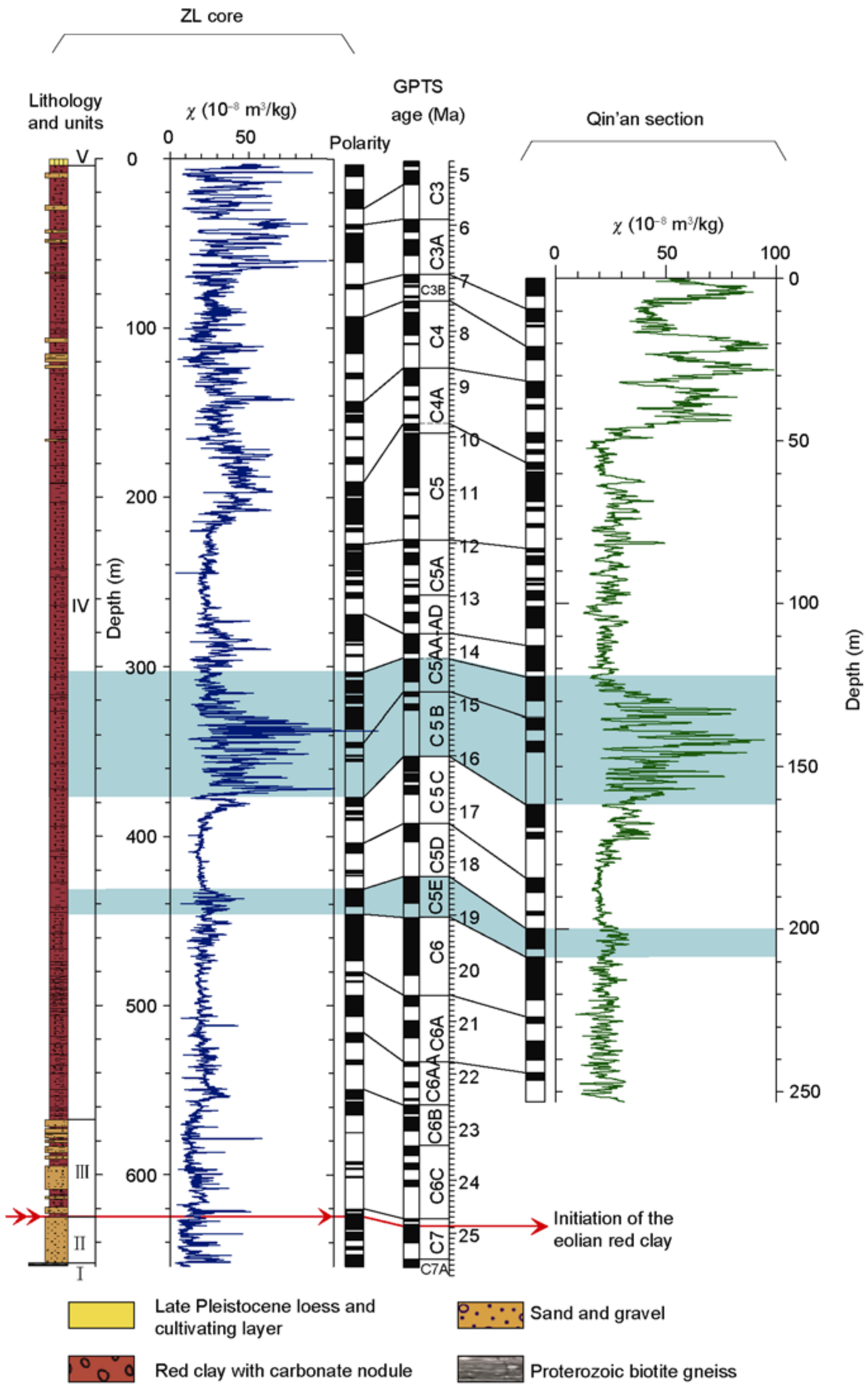

Figure 4 Magnetic susceptibility (χ), magnetostratigraphy of the composite ZL core and their correlation with those of the Qin'an section [41] and the Geomagnetic Polarity Time Scale (GPTS) [46].

but also indicate that they may have generally similar or comparable provenances and dust transport patterns (Figure 5). The earliest eolian red clay layer within the ZL sequence is located at the upper C7n.2n normal chron and has a base age of ca. 25 Ma. This earliest eolian deposit on the CLP thus indicates that developed desert regions have existed in the inland Asia since the late Oligocene epoch. This agrees with the onset of eolian red clay deposits in the Junggar Basin by 24 Ma [42], the increased Asian eolian inputs to the North Pacific at 24–22 Ma [51], and the occurrence of eolian dust in the lacustrine sediments in the Linxia Basin by the late Oligocene [52].

The Quaternary loess-paleosol and late Miocene-Pliocene red clay materials are generally thought to be transported by the northwestward Asian winter monsoon [19, 25, 36]. The Miocene Qin'an red clay is also considered to be

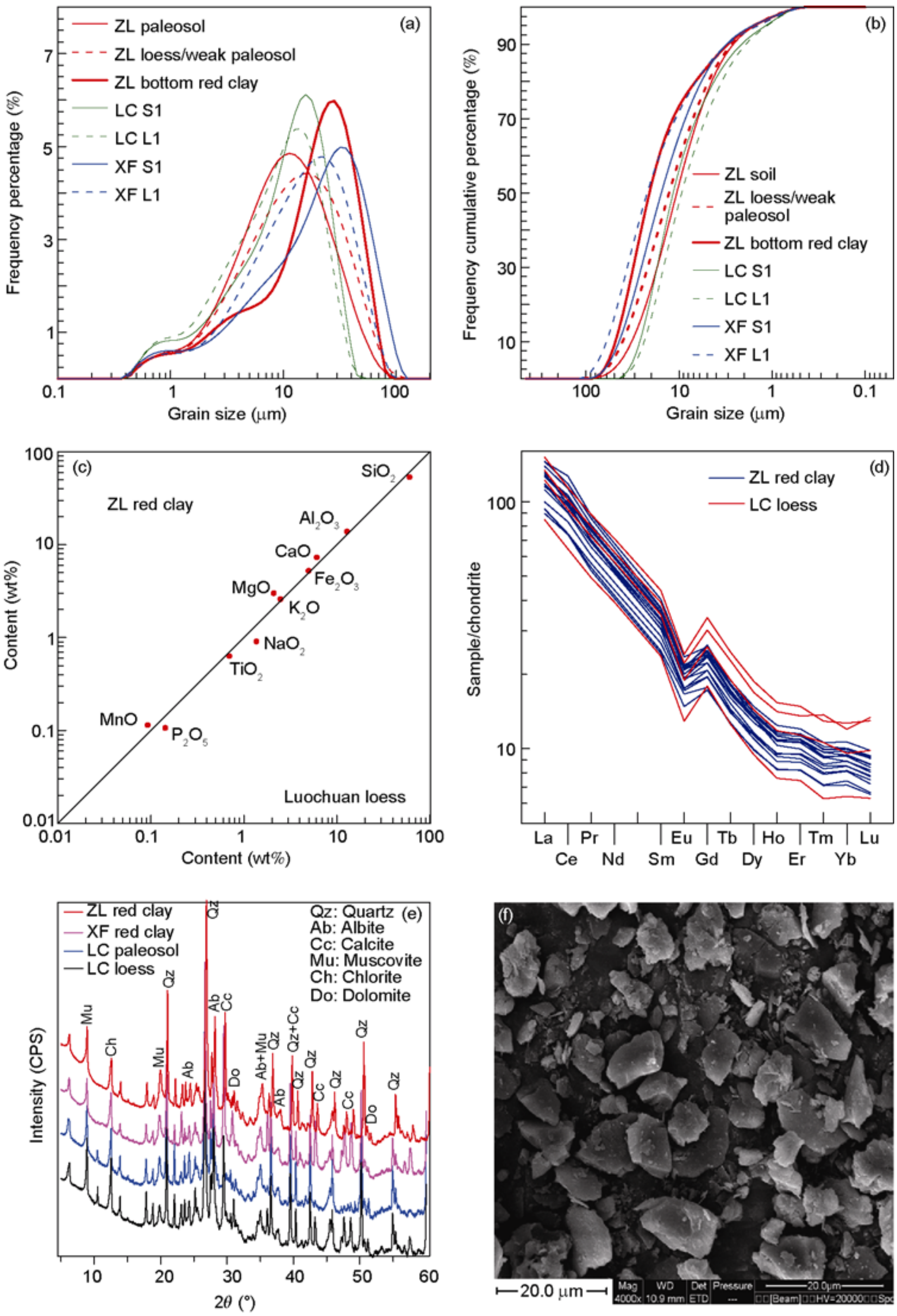

Figure 5 Comparison of grain-size, element, mineral and quartz micromorphology between ZL red clay and Quaternary loess/palesol and Pliocene red clay samples. (a), (b) Averaged grain-size frequency and cumulative percentage distribution of the ZL red clay and the Quaternary loess from the Luochuan (LC) and Xifeng (XF) sections. 5 paleosol and 5 loess/weak paleosol samples from the main portion (30–500 m), 11 paleosol samples from the oldest interval (612.1–624.8 m) of the ZL red clay, 2 loess and 2 paleosol samples from LC L1 and S1, 12 loess and 5 paleosol samples from XF L1 and S1. (c) Major element composition of the ZL red clay and the LC Quaternary loess-soil sequence. (d) Rare-earth element distribution patterns of the ZL red clay (blue lines) and the XF Quaternary loess (red lines). (e) XRD spectrum of selected ZL red clay, LC Quaternary loess/paelsol and XF Pliocene red clay samples. (f) Scanning electronic microscopic (SEM) images of quartz grains from the ZL red clay.

transported by the Asian winter monsoon [41]. However, the red clay in the Junggar Basin, which is more than 2000 km northwest of the Qin'an red clay (Figure 1), is thought to be transported by the westerlies [42]. At present, the ZL areas are jointly influenced by winter monsoon and westerlies in the winter half year. In addition, the overall altitudes of ZL areas are around 2000 m. Therefore, it is plausible that the dust materials of ZL red clay might have been transported by both the winter monsoon and the westerlies.

The initiation of the Asian desertification is one of the most prominent climate changes in Northern Hemisphere during the Cenozoic [53–55]. The uplift of the Tibetan Plateau is suggested to be an important factor that contributes to the desertification of the inland Asia [41, 55, 56]. Uplift of the southern Tibetan Plateau during the late Oligocene [57] would block the transport of moisture from the southern oceans and induce the intensified desertification in the inland Asia [55, 56]. Numerical simulation suggests that the uplift and growth of the Tibetan Plateau from a no-mountain elevation to the present elevation can considerably decrease the precipitation and the humidity in the inland Asia [55, 58]. The retreat of the Paratethys Sea may be another important factor of the Asian desertification [59].

We thank Qinghai Nucleus Industry Geology Bureau for completing the drilling operation; Prof. Zhu Rixiang and Prof. Peter Molnar for discussion and reading an earlier version of this paper; and Zhu Chongshu, Zeng Cheng, Wang Ning and Hou Zhaohua for their field and experiment work assistance. This study was supported by National Basic Research Program of China (Grants Nos. 2010CB833400, 2004CB720200), Innovation Program of Chinese Academy of Sciences (Grant No. KZCX2-YW-Q09-04), National Natural Science Foundation of China (Grants Nos. 41072142, 40921120406 and 40772116) and State Key Laboratory of Loess and Quaternary Geology (SKLLQG).

1 Liu T S, Zhang Z H. Loess of China (in Chinese). Acta Geol Sin, 1962, 42: 1–14
2 Lu Y C, An Z S. The quest for series of nature environmental changes during the Brunhes Epoch (in Chinese). Chin Sci Bull, 1979, 24: 221–224
3 Liu T S, Wen Q Z, Zheng H H, et al. Paleoclimate and its evolution recorded in loess of China (in Chinese). In: Scientific Papers on Geology for International Exchange. Beijing: Geological Publishing House, 1980. 77–82
4 Liu T S. Loess and the Environment. Beijing: China Ocean Press, 1985. 1–481
5 Kukla G, An Z S. Loess stratigraphy in central China. Paleogeogr Paleoclimatol Paleoecol, 1989, 72: 203–233
6 Kukla G, An Z S, Melice J L, et al. Magnetic susceptibility record of Chinese Loess. Trans Royal Soc Edinburgh-Earth Sci, 1990, 81: 263–288
7 Ding Z L, Liu T S. Progresses of loess research in China (part 1): Loess stratigraphy (in Chinese). Quat Sci, 1989, 1: 24–25
8 Heller F, Liu T S. Magnetostratigraphical dating of loess deposits in China. Nature, 1982, 300: 431–433
9 An Z S, Lu Y C. A climatostratigraphic subdivison of late pleistocene strata named by malan formation in north China. Chin Sci Bull, 1984, 29: 1239–1242
10 Sadao S, Wang Y Y. Magneti-and chronostratigraphy revealed from the Luochuan loess sequence in China and its relevance to the Quaternary climatic change. In: Sadao S, Wang Y Y, eds. The Recent Research of Loess in China. Kyoto: Wako Printing Ltd, 1984. 211–230
11 Kukla G, Heller F, Ming L X. Pleistocene climates in China dated by magnetic susceptibility. Geology, 1988, 16: 811–814
12 Ding Z L, Liu T S. Climatic correlation between Chinese loess and deep-sea cores in the last 1.8 Ma. Chin Sci Bull, 1992, 37: 217–220
13 An Z S, Kukla G J, Porter S C, et al. Magnetic susceptibility evidence of monsoon variation on the Loess Plateau of central China during the last 130,000 years. Quat Res, 1991, 36: 29–36
14 An Z S, Kukla G J, Porter S C, et al. Late Quaternary dust flow on the Chinese Loess Plateau. Catena, 1991, 18: 125–132
15 Rutter N, Ding Z L, Evans M E, et al. Baoji-type pedostratigraphic section, Loess Plateau, north-central China. Quat Sci Rev, 1991, 10: 1–22
16 Rutter N W, Ding Z L, Evans M E, et al. Paleoclimates and monsoon variations interpreted from micromorphogenic features of Baoji paleosols, China. Quat Sci Rev, 1993, 12: 853–862
17 Ding Z L, Yu Z W, Rutter N W, et al. Towards an orbital time scale for Chinese loess deposits. Quat Sci Rev, 1994, 13: 39–70
18 An Z S, Liu T S, Lu H Y, et al. The long-term paleomonsoon variation recorded by the loess-paleosol sequence in central China. Quat Inter, 1990, 718: 91–95
19 An Z S, Wu X H, Wang P X, et al. Paleomonsoons of China over the last 130000 years—Paleomonsoon variation. Sci China Ser B, 1991, 34: 1016–1016
20 Sun Y B, Lu H Y, An Z S. Grain-size distribution of quartz isolated from Chinese loess/paleosols. Chin Sci Bull, 2000, 45: 2296–2298
21 Sun Y B, An Z S. Late Pliocene-Pleistocene changes in mass accumulation rates of eolian deposits on the central Chinese Loess Plateau. J Geophys Res, 2005, 110: D23101, doi: 10.1029/ 2005JD006064
22 Liu T S. Loess in China. 2nd ed. Beijing: China Ocean Press; Berlin, Heidelberg: Springer-Verlag, 1988. 1–224
23 Zhao J B. The study on the red soil of Neogene in Xi'an and Baode of Shanxi (in Chinese). Acta Sedimentol Sin, 1989, 7: 113–120
24 Ding Z L, Sun J M, Zhu R X, et al. Eolian origin of the red clay deposits in the Loess Plateau and implications for Pliocene climatic changes (in Chinese). Quat Sci, 1997, 2: 147–157
25 Ding Z L, Sun J M, Liu T S, et al. Wind-blown origin of the Pliocene red clay formation in the central Loess Plateau, China. Earth Planet Sci Lett, 1998, 161: 135–143
26 Lu H Y, Vandenberghe J, An Z S. Aeolian origin and paleoclimatic implications of the 'Red Clay' (North China) as evidenced by grain-size distribution. J Quat Sci, 2001, 16: 89–97
27 Yang S L, Ding Z L. Comparison of particle size characteristics of the Tertiary 'red clay' and Pleistocene loess in the Chinese Loess Plateau: Implications for origin and sources of the 'red clay'. Sedimentology, 2004, 51: 77–93
28 Liu J F, Guo Z T, Qiao Y S, et al. Eolian origin of the Miocene loess-soil sequence at Qin'an, China: Evidence of quartz morphology and quartz grain-size. Chin Sci Bull, 2006, 51: 117–120
29 Qiao Y S, Guo Z T, Hao Q Z, et al. Grain-size features of a Miocene loess-soil sequence at Qinan: Implications on its origin. Sci China Ser D-Earth Sci, 2006, 49: 731–738
30 Li F J, Wu N Q, Pei Y P, et al. Wind-blow origin of Dongwan late Miocene-Pleiocene dust sequence documented by land snail record in western Chinese Loess Plateau. Geology, 2006, 34: 405–408
31 Sun D H, Liu T S, Chen M Y, et al. Magnetostratigraphy and paleoclimate of red Clay sequences from Chinese Loess Plateau. Sci China Ser D-Earth Sci, 1997, 40: 337–343
32 Sun D H, Shaw J, An Z S, et al. Magnetostratigraphy and paleoclimatic interpretation of a continuous 7.2 Ma Late Cenozoic eolian sediments from the Chinese Loess Plateau. Geophys Res Lett, 1998, 25: 85–88
33 Sun D H, An Z S, Shaw J, et al. Magnetostratigraphy and paleoclimatic significance of late Tertiary aeolian sequences in the Chinese Loess Plateau. Geophys J Inter, 1998, 134: 207–212
34 An Z S, Wang S M, Wu X H, et al. Eolian evidence from the Chinese Loess Plateau: The onset of the late Cenozoic Great Glaciation in the Northern Hemispere and Qinghai-Xizang Plateau uplift forcing. Sci Chin Ser D-Earth Sci, 1999, 42: 258–271
35 Ding Z L, Sun J M, Yang S L, et al. Magnetostratigraphy and grain size record of a thick red clay-loess sequence at Lingtai, the Chinese Loess Plateau (in Chinese). Quat Sci, 1998, 1: 86–94
36 Ding Z L, Sun J M, Yang S L, et al. Preliminary magnetostratigraphy of a thick eolian red caly-loess sequence at Lingtai, the Chinese Loess Plateau. Geophys Res Lett, 1998, 25: 1225–1228
37 Ding Z L, Xiong S F, Sun J M, et al. Pedostratigraphy and paleomagnetism of a similar to 7.0 Ma eolian loess-red clay sequence at Lingtai, Loess Plateau, north-central China and the implications for

paleomonsoon evolution. Palaeogeogr Palaeoclimatol Palaeoecol, 1999, 152: 49–66
38 Song Y G, Fang X M, Torii M, et al. Late Neogene rock magnetic record of climatic variation from Chinese eolian sediments related to the uplift of the Tibetan Plateau. J Asian Earth Sci, 2007, 30: 324–332
39 Qiang X K, Li Z X, Powell C McA, et al. Magnetostratigraphic record of the Late Miocene onset of the East Asian monsoon, and Pliocene uplift of northern Tibet. Earth Planet Sci Lett, 2001, 187: 83–93
40 Xu Y, Yue L P, Li J X, et al. An 11-Ma-old red clay sequence on the Eastern Chinese Loess Plateau. Paleogeogr Paleoclimatol Paleoecol, 2009, 284: 383–391
41 Guo Z T, Ruddiman W F, Hao Q Z, et al. Onset of Asian desertification by 22 Myr ago inferred from loess deposits in China. Nature, 2002, 416: 159–163
42 Sun J M, Ye J, Wu W Y, et al. Late Oligocene-Miocene mid-latitude aridification and wind patterns in the Asian interior. Geology, 2010, 38: 515–518
43 Qiang X K, An Z S, Fu C F, et al. Magnetostratigraphy of Zhuanglang drilling core from western Loess Plateau. The 5th International Symposium on Tibetan Plateau & the 24th Himalaya-Karakorum-Tibet Workshop. 11–14 August 2009, Beijing, China, 2009. S2.7, 69
44 Zijderveld J D A. AC demagnetization of rocks: Analysis of results. In: Collinson D W, Runcorn S K, Creer K M, eds. Methods in Paleomagnetism. New York: Elsevier, 1967. 254–286
45 Kirschvink J L. The least-squares line and plane and the analysis of paleomagnetic data. Geophys J Roy Astron Soc, 1980, 62: 699–718
46 Cande S C, Kent D V. Revised calibration of the geomagnetic polarity timescale for the late Cretaceous and Cenozoic. J Geophys Res, 1995, 100: 6093–6095
47 Liu J F, Guo Z T, Qiao Y S, et al. Eolian origin of the Miocene loess-soil sequence at Qin'an, China: Evidence of quartz morphology and quartz grain-size. Chin Sci Bull, 2006, 51: 117–120
48 Ding Z L, Rutter N W, Sun J M, et al. Re-arrangement of atmospheric circulation at about 2.6 Ma over northern China: Evidence from grain size records of loess-palaeosol and red clay sequences. Quat Sci Rev, 2000, 19: 547–558
49 Sun J M. Provenance of loess material and formation of loess deposits on the Chinese Loess Plateau. Earth Planet Sci Lett, 2002, 203: 845–859
50 Guo Z T, Sun B, Zhang Z S, et al. A major reorganization of Asian climate by the early Miocene. Clim Past, 2008, 4: 153–174
51 Rea D K, Leinen M, Janecek T R. Geologic approach to the long-term history of atmospheric circulation. Science, 1985, 227: 721–725
52 Garzione C N, Ikari M J, Basu A R. Source of Oligocene to Pliocene sedimentary rocks in the Linxia Basin in northeastern Tibet from Nd isotopes: Implications for tectonic forcing of climate. Geol Soc Amer Bull, 2006, 117: 1156–1166
53 Ruddimman W F, Kutzbach J K. Forcing of late Cenozoic northern hemisphere climate by plateau uplift in southern Asia and American West. J Geophys Res, 1989, 94: 18409–18427
54 Manabe S, Broccoli A J. Mountains and arid climates of middle latitudes. Science, 1990, 247: 192–195
55 An Z S, Kutzbach J E, Prell W L, et al. Evolution of Asian monsoons and phased uplift of the Himalayan Tibetan Plateau since Late Miocene times. Nature, 2001, 411: 62–66
56 Kutzbach J E, Guetter P J, Ruddimman W F, et al. Senseitivity of climate to Late Cenozoic uplift in southern Asia and the American West: Numerical experiments. J Geophys Res, 1989, 94: 18393–18407
57 Harrison T M, Copeland P, Kidd W S F, et al. Raising Tibet. Science, 1992, 255: 1663–1670
58 Kutzbach J E, Prell W L, Ruddimman W F. Sensitivity of Eurasian climate to surface uplift of the Tibetan Plateau. J Geol, 1993, 101: 177–190
59 Ramstein G, Fluteau F, Besse J, et al. Effect of orogeny, plate motion and land-sea distribution on Eurasian climate change over the past 30 million years. Nature, 1997, 386: 788–795